High-capacity rechargeable batteries based on deeply cyclable lithium metal anodes

Qiuwei Shi[a,b,1], Yiren Zhong[a,1], Min Wu[a,1], Hongzhi Wang[b,2], and Hailiang Wang[a,2]

[a]Department of Chemistry and Energy Sciences Institute, Yale University, West Haven, CT 06516; and [b]State Key Laboratory for Modification of Chemical Fibers and Polymer Materials, Donghua University, 201620 Shanghai, People's Republic of China

Edited by Thomas E. Mallouk, The Pennsylvania State University, University Park, PA, and approved April 13, 2018 (received for review February 28, 2018)

Discovering new chemistry and materials to enable rechargeable batteries with higher capacity and energy density is of paramount importance. While Li metal is the ultimate choice of a battery anode, its low efficiency is still yet to be overcome. Many strategies have been developed to improve the reversibility and cycle life of Li metal electrodes. However, almost all of the results are limited to shallow cycling conditions (e.g., 1 mAh cm^{-2}) and thus inefficient utilization (<1%). Here we achieve Li metal electrodes that can be deeply cycled at high capacities of 10 and 20 mAh cm^{-2} with average Coulombic efficiency >98% in a commercial $LiPF_6$/carbonate electrolyte. The high performance is enabled by slow release of $LiNO_3$ into the electrolyte and its subsequent decomposition to form a Li_3N and lithium oxynitrides (LiN_xO_y)-containing protective layer which renders reversible, dendrite-free, and highly dense Li metal deposition. Using the developed Li metal electrodes, we construct a Li-MoS_3 full cell with the anode and cathode materials in a close-to-stoichiometric amount ratio. In terms of both capacity and energy, normalized to either the electrode area or the total mass of the electrode materials, our cell significantly outperforms other laboratory-scale battery cells as well as the state-of-the-art Li ion batteries on the market.

lithium metal anode | deep cycling | high capacity | high energy | lithium metal battery

Rechargeable batteries with high energy density are of paramount importance to energy storage. The progress of high-performance batteries is heavily dependent on the development of new chemistries and materials (1–9). With a high theoretical capacity (3,860 mAh g^{-1}), a low redox potential (−3.040 V vs. the standard hydrogen electrode), and a light weight (0.53 g cm^{-3}), Li metal is the ultimate choice of anode for Li-based and perhaps all rechargeable batteries (10–15). However, major challenges must be overcome before rechargeable Li metal batteries become viable. The foremost is the low degree of utilization of Li, poor reversibility, and dendrite formation during cycling, which is responsible for phenomena such as low Coulombic efficiency (CE), large voltage polarization, poor capacity retention, and short-circuiting, and leads to early failure and critical safety concerns for the batteries (11, 16–18). This problem is especially severe for carbonate-based electrolyte, which is the electrolyte for all commercial Li ion batteries (LIBs). Another obstacle is the lack of a high-capacity cathode material that can be paired with Li metal in carbonate electrolyte.

Many strategies, such as superconcentrated electrolytes (19, 20), electrolyte additives based on fluorinated, nitrogenous, and polysulfide compounds (21, 22), artificial solid electrolyte interphase (SEI) structures (23, 24), separator modification with metal-organic frameworks and nanocarbon (25, 26), and anode structures for hosting Li metal (27–29), have been demonstrated to be effective in improving the efficiency and cycle life of Li metal electrodes. However, thus far almost all of the electrochemical measurements on Li metal electrodes have been limited to shallow cycling (10, 16, 17, 23, 24, 28, 30, 31). For instance, an electrode containing more than 100 mAh cm^{-2} of Li is only charged and discharged to the depth of 1 mAh cm^{-2}. Similarly, for full cells of Li metal batteries, a cathode is often paired with a Li metal anode that is in large excess (12, 26, 31), and as a result neither the capacity nor cycling stability reflects the real full-cell performance. It is thus critical to develop deeply cyclable Li metal electrodes and further realize high-capacity Li metal full cells based on cathode and anode materials in stoichiometric ratios.

Here we report Li metal electrodes that can be deeply cycled at high capacities of 10 and 20 mAh cm^{-2} with average CE >98% in a commercial $LiPF_6$/carbonate electrolyte. The high-performance electrodes are enabled by slow release and decomposition of $LiNO_3$ preimpregnated in the separator membrane, which forms a micrometer-thick protective layer with Li_3N and lithium oxynitrides (LiN_xO_y) as the major active components and renders reversible, dendrite-free, and highly dense Li metal deposition. Using the developed Li metal electrodes, we construct a Li-MoS_3 full cell with the anode (Li) and cathode (MoS_3) materials in a close-to-stoichiometric amount ratio. Based on the total mass of the electrode materials, the cell delivers a specific capacity of 410 mAh g^{-1} and an areal capacity of 6.3 mAh cm^{-2}. In terms of both capacity and energy, our cell significantly outperforms other laboratory-scale battery cells, including Li metal or Si-based ones, as well as the state-of-the-art LIBs on the market.

Results and Discussion

While $LiNO_3$ is often used as an additive for the ether-based electrolyte (highly volatile and inflammable) specific for Li-S

Significance

Lithium metal is considered as the ultimate choice of anode for high-energy batteries, but the existing Li metal electrodes are usually limited to shallow cycling conditions (1 mAh cm^{-2}) and thus inefficient utilization (<1%). We achieve Li metal electrodes deeply and stably cyclable to capacities >10 mAh cm^{-2}, enabled by slow release of $LiNO_3$ into carbonate electrolyte and its subsequent decomposition to form a protective layer for reversible, dendrite-free, and highly dense Li metal deposition. Based on that, we demonstrate a Li-MoS_3 (in close-to-stoichiometric ratio) cell showing high areal and specific capacity and energy.

Author contributions: Q.S., Y.Z., M.W., and Hailiang Wang designed research; Q.S., Y.Z., and M.W. performed research; Q.S., Y.Z., and M.W. analyzed data; and Q.S., Y.Z., Hongzhi Wang, and Hailiang Wang wrote the paper.

The authors declare no conflict of interest.

This article is a PNAS Direct Submission.

[1]Q.S., Y.Z., and M.W. contributed equally to this work.

[2]To whom correspondence may be addressed. Email: hailiang.wang@yale.edu or wanghz@dhu.edu.cn.

This article contains supporting information online at www.pnas.org/lookup/suppl/doi:10.1073/pnas.1803634115/-/DCSupplemental.

Published online May 14, 2018.

batteries, it has rarely been used to protect Li metal electrodes working with the general and more desirable carbonate-based electrolyte (32). A possible reason is that $LiNO_3$ is insoluble ($\sim 10^{-5}$ g mL^{-1}) in the carbonate solvent. In this work, we find that $LiNO_3$ can greatly improve the performance of Li metal electrodes via a slow release and decomposition scheme. We immersed a glass fiber separator in a $LiNO_3$ solution to impregnate the separator with submicrometer-scale crystallites of $LiNO_3$ (*SI Appendix*, Figs. S1–S3). Under working conditions, the crystallites can serve as a reservoir for the limited amount of $LiNO_3$ dissolved in the electrolyte to decompose and form a protective layer on the Li metal electrode.

We assembled Li||Cu cells with pristine and $LiNO_3$-modified separators to investigate the electrochemical Li plating/stripping processes. A commercial electrolyte based on 1 M $LiPF_6$ in an ethylene carbonate/diethyl carbonate (1:1 volumetric ratio) mixed solvent was used. The CE of a cell, defined as the ratio of the amount of the stripped Li to that of the plated Li on the Cu current collector in each charging–discharging cycle, was used as a performance index to evaluate the cyclability of the Li metal electrode. At the current density of 1 mA cm^{-2}, the cells with $LiNO_3$ could be stably cycled for 210 and 160 cycles with average CEs of 95.1% and 98.3% to the capacity depths of 2 and 5 mAh cm^{-2} (Fig. 1 *A* and *B*), respectively. Under even harsher conditions of 2 mA cm^{-2}–5 mAh cm^{-2} and 5 mA cm^{-2}–10 mAh cm^{-2}, the cells with $LiNO_3$ could work stably for 100 and 50 cycles with high average CEs of 96.8% and 98.1% (Fig. 1 *C* and *D*), respectively. In contrast, the cells without $LiNO_3$ exhibited substantially worse cycling performance (Fig. 1 *A*–*D*). Only 30 cycles with an average CE of 91.6% could be obtained under the 1 mA cm^{-2}–2 mAh cm^{-2} conditions. At the 5 mA cm^{-2}–10 mAh cm^{-2} conditions, the cell was not even cyclable. The corresponding charging–discharging voltage profiles are plotted in *SI Appendix*, Figs. S4 and S5. The CEs and voltage profiles of the Li||Cu cells with and without $LiNO_3$ cycled at other current–capacity conditions (1 mA cm^{-2}–1 mAh cm^{-2}, 2 mA cm^{-2}–1 mAh cm^{-2}, 4 mA cm^{-2}–1 mAh cm^{-2}, 1 mA cm^{-2}–10 mAh cm^{-2}, 2 mA cm^{-2}–10 mAh cm^{-2}, and 5 mA cm^{-2}–5 mAh cm^{-2}) are shown in *SI Appendix*, Figs. S6–S11. Fig. 1*E* compares the performance indices of our $LiNO_3$-protected Li metal electrodes with those reported in the literature for other Li metal electrodes in the Li||Cu configuration based on carbonate electrolyte. It is evident that our electrodes can achieve much higher capacities (i.e., can be much more deeply cycled) and rate capability without compromising other properties such as the CE and cycle life.

We analyzed the dependence of CE on current and capacity for the Li||Cu cells with $LiNO_3$. As the charging–discharging current increases from 1 to 4 mA cm^{-2}, the CE decreases from 93.7% to 91.2% at a fixed cycling capacity of 1 mAh cm^{-2} (*SI Appendix*, Fig. S12*A*). This is consistent with literature precedence and the general knowledge that chemical reactions are less reversible at higher rates. *SI Appendix*, Fig. S12*B* shows the dependence of CE on charging–discharging capacity at various current densities. At each current density, the CE increases with the capacity. This is also confirmed by control experiments in which the charging–discharging current density for a Li||Cu cell is increased or decreased stepwise (*SI Appendix*, Fig. S13). Despite not being straightforward, similar phenomena have actually been observed before and indicate that the nucleation or initial growth stage is less reversible than the subsequent Li deposition (33–35).

We used scanning electron microscopy (SEM) to image the Li deposited on the Cu current collector after deep cycling. After the Li plating step in the third cycle under the demanding 5 mA cm^{-2}–10 mAh cm^{-2} conditions, the deposited Li of the Li||Cu cell without $LiNO_3$ manifests a loosely packed structure consisted of dendrites and whiskers (Fig. 2*A*). Further cycling

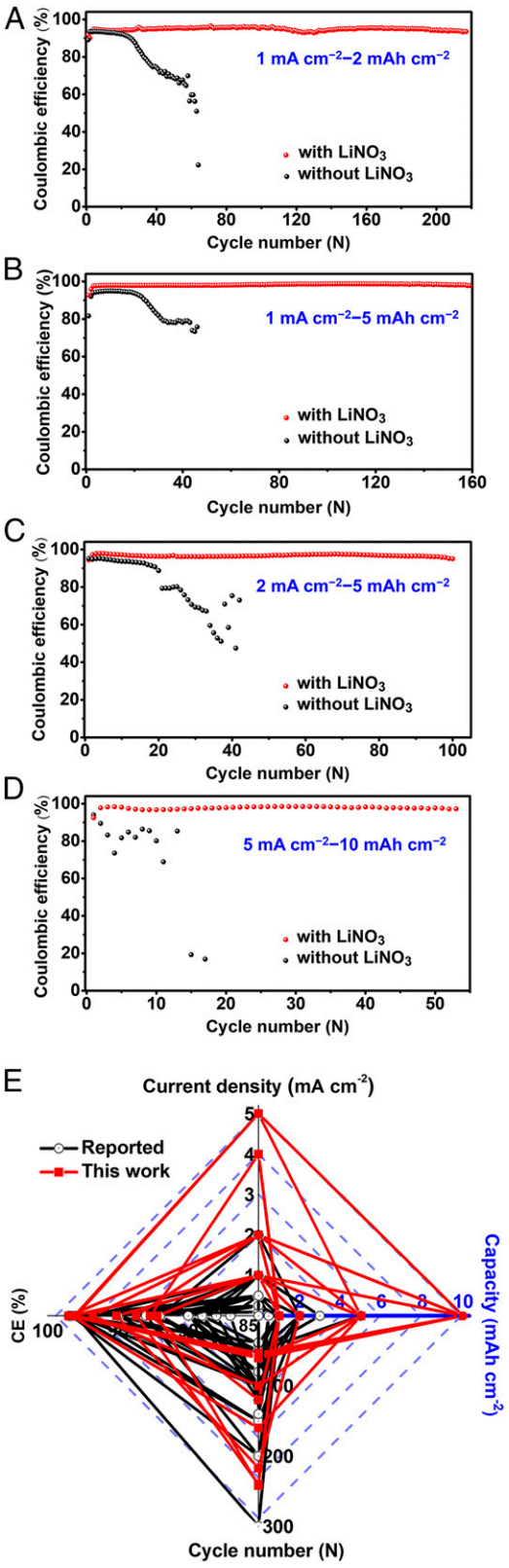

Fig. 1. CE of Li||Cu cells with and without $LiNO_3$ cycled under (*A*) 1 mA cm^{-2}–2 mAh cm^{-2}, (*B*) 1 mA cm^{-2}–5 mAh cm^{-2}, (*C*) 2 mA cm^{-2}–5 mAh cm^{-2}, and (*D*) 5 mA cm^{-2}–10 mAh cm^{-2} conditions. (*E*) Comparison in electrochemical performance indices (capacity, current density, CE, and cycle number), as measured in the Li||Cu configuration based on carbonate electrolyte, of our $LiNO_3$-protected Li metal electrodes with those reported in the literature (a total of 27 entries as summarized in *SI Appendix*, Table S1).

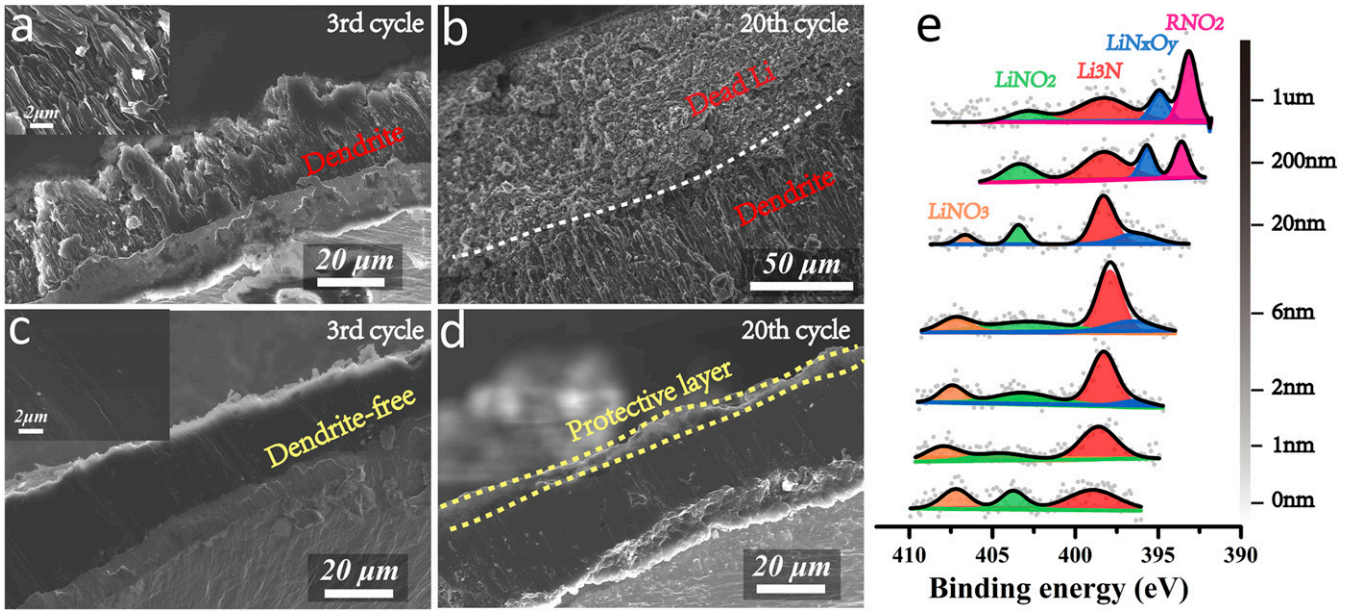

Fig. 2. Cross-section SEM images of the Li layer plated on the Cu current collector after 3 and 20 cycles under 2 mA cm^{-2}–10 mAh cm^{-2} conditions for the Li||Cu cells (*A* and *B*) without and (*C* and *D*) with $LiNO_3$. (*Insets*) Enlarged images of the corresponding cross-sections of the Li layers. (*E*) N 1s XPS spectra at various depths of the plated Li layer on the Cu current collector after three cycles under 2 mA cm^{-2}–10 mAh cm^{-2} conditions for the Li||Cu cell with $LiNO_3$.

continues to expand the unstable SEI and deteriorate the electrode structure, resulting in an ∼100-μm-thick dendritic Li layer covered with another ∼100-μm-thick mossy C-containing Li layer after 20 cycles (Fig. 2*B* and *SI Appendix*, Fig. S14). In stark contrast, the deposited Li of the Li||Cu cell with $LiNO_3$ displays an ∼40 μm-thick dense and uniform film structure without any traces of dendrites (Fig. 2*C*). The structure and thickness of the Li layer could still be maintained after 20 cycles (Fig. 2*D*). We note an ∼2-μm-thick layer with a porous surface morphology (*SI Appendix*, Fig. S15) on the surface of the plated Li layer (Fig. 2*D*), which is likely the protective layer formed by the decomposition of $LiNO_3$.

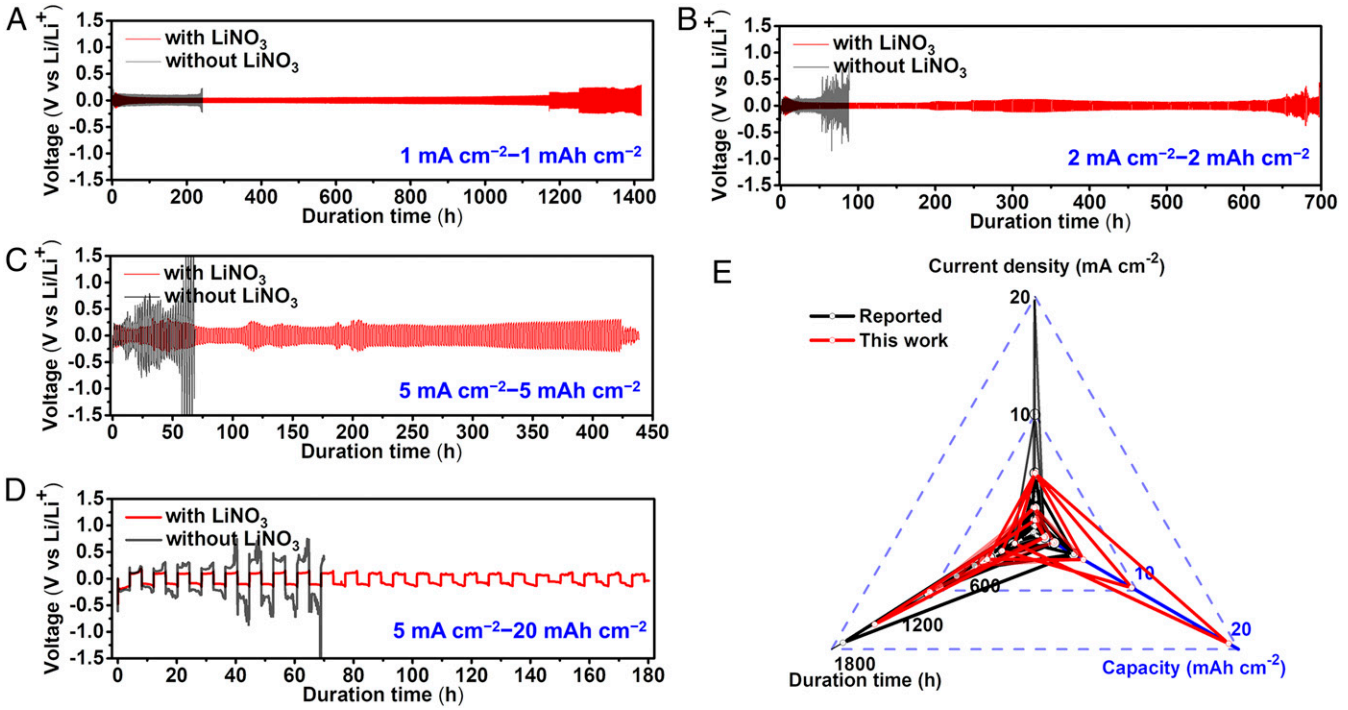

Fig. 3. Cycling performance of Li||Li symmetric cells with and without $LiNO_3$ cycled under (*A*) 1 mA cm^{-2}–1 mAh cm^{-2}, (*B*) 2 mA cm^{-2}–2 mAh cm^{-2}, (*C*) 5 mA cm^{-2}–5 mAh cm^{-2}, and (*D*) 5 mA cm^{-2}–20 mAh cm^{-2} conditions; (*E*) Comparison of electrochemical performance indices (capacity, current density, and duration time), as measured in the Li||Li configuration based on carbonate electrolyte, of our $LiNO_3$-protected Li metal electrodes with those reported in the literature (a total of 32 entries as summarized in *SI Appendix*, Table S2).

We then resorted to X-ray photoelectron spectroscopy (XPS) to analyze the chemical composition of the $LiNO_3$-derived protective layer. Thickness-dependent elemental compositions, together with the corresponding C 1s, O 1s, and Li 1s XPS spectra, are shown in *SI Appendix*, Figs. S16–S19 for the Li-plated Cu electrodes of the Li||Cu cells with and without $LiNO_3$ after three cycles under the 2 mA cm^{-2}–10 mAh cm^{-2} conditions. Both electrodes possess an SEI featuring an outer surface rich in lithium semicarbonates (ROCOOLi) and Li_2CO_3, and an inner layer dominated by Li_2O, consistent with the prevalent "mosaic model" (36, 37). It is worth noting that the C content on the $LiNO_3$-free electrode decreases with the sputtering thickness significantly more slowly than that on the $LiNO_3$-protected electrode (*SI Appendix*, Fig. S16), indicating more severe electrolyte decomposition on the electrode surface without a $LiNO_3$-derived protective layer. Since the two electrodes contain similar C and O species in the surface layer, we attribute the desirable functionalities of the $LiNO_3$-derived protective layer to the *N*-containing species. Fig. 2*E* plots the depth-dependent N 1s XPS spectra for the $LiNO_3$-protected electrode. The major components of the protective layer are Li_3N, LiN_xO_y, $LiNO_2$, and alkyl nitro species (R-NO_2). Both Li_3N and LiN_xO_y are known to be good Li ion conductors and can promote efficient and stable cycling of Li metal electrodes (38, 39), which is also supported by the stabilized Li ion transfer resistance for the Li||Cu cell with $LiNO_3$ upon cycling (*SI Appendix*, Fig. S20).

We also fabricated symmetric Li||Li cells to evaluate the electrochemical performance of our $LiNO_3$-protected Li metal electrodes. At the charging–discharging current density of 1 mA cm^{-2} and capacity of 1 mAh cm^{-2}, the Li||Li cell with $LiNO_3$ could be stably cycled for 1,400 h with an average overpotential of 80 mV (Fig. 3*A*). It could be functional for 700 h under the 2 mA cm^{-2}–2 mAh cm^{-2} conditions, showing an overpotential of 84 mV (Fig. 3*B*). Under the demanding conditions of 5 mA cm^{-2}–5 mAh cm^{-2}, the cell could be stably cycled for 420 h with an average overpotential of 192 mV (Fig. 3*C*). The Li||Li cell with $LiNO_3$ could even be cycled to an extremely high capacity of 20 mAh cm^{-2} (Fig. 3*D*). The cycling performance under other conditions (2 mA cm^{-2}–1 mAh cm^{-2}, 2 mA cm^{-2}–5 mAh cm^{-2}, and 5 mA cm^{-2}–10 mAh cm^{-2}) is given in *SI Appendix*, Fig. S21. Under all conditions, the Li||Li cells without $LiNO_3$ exhibited much worse performance (Fig. 3 and *SI Appendix*, Fig. S21). Fig. 3*E* compares the performance indices of our $LiNO_3$-protected Li metal electrodes with those reported in the literature for other Li metal electrodes in the Li||Li configuration based on carbonate electrolyte. It is evident that our electrodes can achieve much higher capacities without sacrificing other properties such as the CE, cycle life and rate capability.

As a proof of concept, we utilized our $LiNO_3$-protected Li metal electrodes to fabricate close-to-stoichiometric full cells with ultrahigh capacity and energy. We chose amorphous MoS_3 as the cathode material because of its proven high capacity and compatibility with carbonate electrolyte (40–43). Our MoS_3 grown on mildly oxidized carbon nanotubes (CNTs) (*SI Appendix*, Fig. S22) exhibits a specific capacity of ∼500 mAh g^{-1} at the current density of 0.7 mA cm^{-2} and a mass loading of 12.5 mg cm^{-2} (*SI Appendix*, Fig. S23). To assemble the full cell (Fig. 4*A*), we paired a predeposited $LiNO_3$-protected Li metal electrode (10 mAh cm^{-2}, 2.6 mg cm^{-2}) with a MoS_3 electrode (∼6.4 mAh cm^{-2}, 12.8 mg cm^{-2}). The full cell delivered an areal capacity of 6.3 mAh cm^{-2}, corresponding to a specific capacity of 410 mAh g^{-1} based on the total mass of electrode materials (Fig. 4*B*). Coupled with the average discharging voltage of 1.95 V, the cell afforded an areal energy of 12.2 Wh cm^{-2} and a specific energy of 793 Wh kg^{-1} based on the total mass of electrode materials. Both the capacity and energy of our Li-MoS_3 full cell, normalized to either the electrode area or the total mass of both the anode and cathode materials, are significantly higher than other Li battery cells, including the previously reported high-capacity cells based on Li metal or Si (29, 44–46), as well as the state-of-the-art Li ion batteries on the market (Fig. 4 *C* and *D*), putting forward a competitive candidate for future-generation high-capacity and high-energy rechargeable batteries. However, the cycling stability of the full cell is still poor, which is ascribed to the capacity fading of both electrodes. Specific energy of the cell can be further improved if a new cathode material with a comparable capacity and a higher operating potential can be developed.

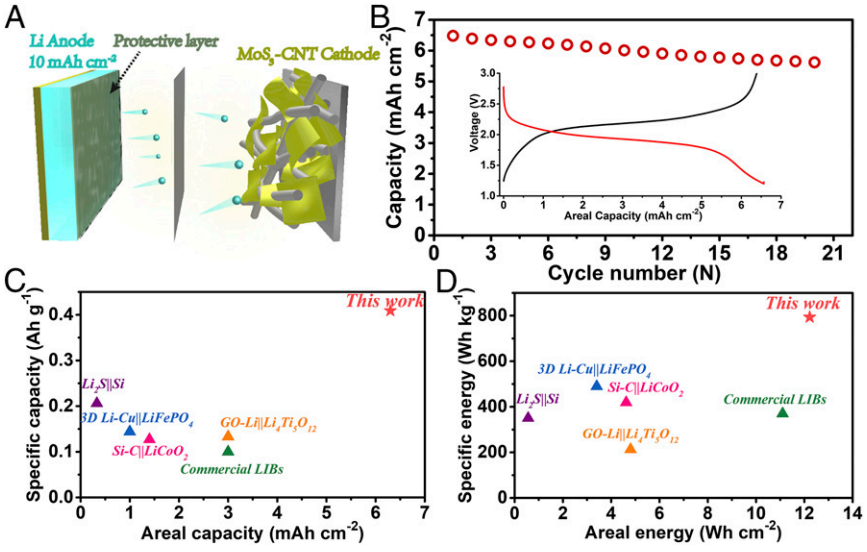

Fig. 4. (*A*) Schematic structure and (*B*) charging–discharging voltage profiles and cycling performance of the close-to-stoichiometric Li-MoS_3 cell. Comparisons in (*C*) specific and areal capacity and (*D*) specific and areal energy of our Li-MoS_3 cell with other full cells reported in the literature. All of the numbers are normalized to the total mass of anode and cathode materials excluding conductive carbon black and binder. Carbon-host materials such as the mesoporous carbon for Li_2S in the Li_2S||Si case and the CNTs for MoS_3 in this work are included in the calculation for total mass. The values for commercials LIBs are calculated based on a $LiCoO_2$ cathode (20 mg cm^{-2}, 150 mAh g^{-1}) paired with a graphite anode (10 mg cm^{-2}, 300 mAh g^{-1}).

In summary, by forming a protective SEI layer under slow release of $LiNO_3$ into a commercial carbonate electrolyte solution, we have enabled high-performance Li metal electrodes deeply cyclable to high capacities of 10 or 20 mAh cm^{-2}. Based on the $LiNO_3$-protected Li metal electrodes, we have successfully constructed close-to-stoichiometric Li-MoS_3 full cells with ultrahigh specific and areal capacity and energy.

Materials and Methods

Materials and methods, additional characterizations, electrochemical data, and tables for performance comparison are available in *SI Appendix*.

ACKNOWLEDGMENTS. This work was partially supported by Yale University. Q.S. acknowledges the support from China Scholarship Council. Hongzhi Wang acknowledges the support from Programs of 16JC1400700, 2017-01-07-00-03-E00055, 16XD1400100, and Eastern Scholar.

1. Suo L, et al. (2015) "Water-in-salt" electrolyte enables high-voltage aqueous lithium-ion chemistries. *Science* 350:938–943.
2. Lim J, et al. (2016) Origin and hysteresis of lithium compositional spatiodynamics within battery primary particles. *Science* 353:566–571.
3. Zhu Z, et al. (2016) Anion-redox nanolithia cathodes for Li-ion batteries. *Nat Energy* 1: 16111.
4. Gao X, Chen Y, Johnson LR, Jovanov ZP, Bruce PG (2017) A rechargeable lithium–oxygen battery with dual mediators stabilizing the carbon cathode. *Nat Energy* 2: 17118.
5. Grey CP, Tarascon JM (2016) Sustainability and in situ monitoring in battery development. *Nat Mater* 16:45–56.
6. Sun H, et al. (2017) Three-dimensional holey-graphene/niobia composite architectures for ultrahigh-rate energy storage. *Science* 356:599–604.
7. Rustomji CS, et al. (2017) Liquefied gas electrolytes for electrochemical energy storage devices. *Science* 356:1351.
8. Bai S, Liu X, Zhu K, Wu S, Zhou H (2016) Metal–organic framework-based separator for lithium–sulfur batteries. *Nat Energy* 1:16094.
9. Dunn B, Kamath H, Tarascon J-M (2011) Electrical energy storage for the grid: A battery of choices. *Science* 334:928–935.
10. Liang X, et al. (2017) A facile surface chemistry route to a stabilized lithium metal anode. *Nat Energy* 2:17119–17124.
11. Tikekar MD, Choudhury S, Tu Z, Archer LA (2016) Design principles for electrolytes and interfaces for stable lithium-metal batteries. *Nat Energy* 1:16114.
12. Zheng J, et al. (2017) Electrolyte additive enabled fast charging and stable cycling lithium metal batteries. *Nat Energy* 2:17012.
13. Liu T, et al. (2015) Cycling Li-O_2 batteries via LiOH formation and decomposition. *Science* 350:530–533.
14. Lu J, et al. (2016) A lithium-oxygen battery based on lithium superoxide. *Nature* 529: 377–382.
15. Albertus P, Babinec S, Litzelman S, Newman A (2018) Status and challenges in enabling the lithium metal electrode for high-energy and low-cost rechargeable batteries. *Nat Energy* 3:16–21.
16. Cheng XB, Zhang R, Zhao CZ, Zhang Q (2017) Toward safe lithium metal anode in rechargeable batteries: A review. *Chem Rev* 117:10403–10473.
17. Lin D, Liu Y, Cui Y (2017) Reviving the lithium metal anode for high-energy batteries. *Nat Nanotechnol* 12:194–206.
18. Yang C, Fu K, Zhang Y, Hitz E, Hu L (2017) Protected lithium-metal anodes in batteries: From liquid to solid. *Adv Mater* 29:1701169.
19. Qian J, et al. (2015) High rate and stable cycling of lithium metal anode. *Nat Commun* 6:6362.
20. Suo L, Hu Y-S, Li H, Armand M, Chen L (2013) A new class of solvent-in-salt electrolyte for high-energy rechargeable metallic lithium batteries. *Nat Commun* 4:1481.
21. Cheng X-B, et al. (2017) Implantable solid electrolyte interphase in lithium-metal batteries. *Chem* 2:258–270.
22. Lu Y, Tu Z, Archer LA (2014) Stable lithium electrodeposition in liquid and nanoporous solid electrolytes. *Nat Mater* 13:961–969.
23. Zhu B, et al. (2017) Poly(dimethylsiloxane) thin film as a stable interfacial layer for high-performance lithium-metal battery anodes. *Adv Mater* 29:1603755.
24. Gao Y, et al. (2017) Interfacial chemistry regulation via a skin-grafting strategy enables high-performance lithium-metal batteries. *J Am Chem Soc* 139:15288–15291.
25. Liu W, et al. (2017) Functional metal-organic framework boosting lithium metal anode performance via chemical interactions. *Chem Sci (Camb)* 8:4285–4291.
26. Liu Y, et al. (2017) Making Li-metal electrodes rechargeable by controlling the dendrite growth direction. *Nat Energy* 2:17083–17093.
27. Li Q, Zhu S, Lu Y (2017) 3D porous Cu current collector/Li-metal composite anode for stable lithium-metal batteries. *Adv Funct Mater* 27:1606422.
28. Zhang Y, et al. (2017) High-capacity, low-tortuosity, and channel-guided lithium metal anode. *Proc Natl Acad Sci USA* 114:3584–3589.
29. Lin D, et al. (2016) Layered reduced graphene oxide with nanoscale interlayer gaps as a stable host for lithium metal anodes. *Nat Nanotechnol* 11:626–632.
30. Choudhury S, et al. (2017) Electroless formation of hybrid lithium anodes for fast interfacial ion transport. *Angew Chem Int Ed Engl* 56:13070–13077.
31. Cheng XB, et al. (2017) Nanodiamonds suppress the growth of lithium dendrites. *Nat Commun* 8:336.
32. Guo J, Wen Z, Wu M, Jin J, Liu Y (2015) Vinylene carbonate–LiNO3: A hybrid additive in carbonic ester electrolytes for SEI modification on Li metal anode. *Electrochem Commun* 51:59–63.
33. Li W, et al. (2015) The synergetic effect of lithium polysulfide and lithium nitrate to prevent lithium dendrite growth. *Nat Commun* 6:7436.
34. Liu W, et al. (2017) Core-shell nanoparticle coating as an interfacial layer for dendrite-free lithium metal anodes. *ACS Cent Sci* 3:135–140.
35. Adams BD, Zheng J, Ren X, Xu W, Zhang J-G (2017) Accurate determination of Coulombic efficiency for lithium metal anodes and lithium metal batteries. *Adv Energy Mater* 8:1702097.
36. Peled E (1997) Advanced model for solid electrolyte interphase electrodes in liquid and polymer electrolytes. *J Electrochem Soc* 144:L208–L210.
37. Peled E, Menkin S (2017) Review—SEI: Past, present and future. *J Electrochem Soc* 164:A1703–A1719.
38. Li L, et al. (2016) Origins of large voltage hysteresis in high-energy-density metal fluoride lithium-ion battery conversion electrodes. *J Am Chem Soc* 138:2838–2848.
39. Wang F, et al. (2012) Tracking lithium transport and electrochemical reactions in nanoparticles. *Nat Commun* 3:1201.
40. Jacobson AJ, Chianelli RR, Rich SM, Whittingham MS (1979) Amorphous molybdenum trisulfide: A new lithium battery cathode. *Mater Res Bull* 14:1437–1448.
41. Doan-Nguyen VVT, et al. (2016) Molybdenum polysulfide chalcogels as high-capacity, anion-redox-driven electrode materials for Li-ion batteries. *Chem Mater* 28: 8357–8365.
42. Matsuyama T, et al. (2016) Structure analyses using X-ray photoelectron spectroscopy and X-ray absorption near edge structure for amorphous MS 3 (M: Ti, Mo) electrodes in all-solid-state lithium batteries. *J Power Sources* 313:104–111.
43. Ye H, et al. (2017) Amorphous MoS_3 as the sulfur-equivalent cathode material for room-temperature Li-S and Na-S batteries. *Proc Natl Acad Sci USA* 114:13091–13096.
44. Yang C-P, Yin Y-X, Zhang S-F, Li N-W, Guo Y-G (2015) Accommodating lithium into 3D current collectors with a submicron skeleton towards long-life lithium metal anodes. *Nat Commun* 6:8058.
45. Yang Y, et al. (2010) New nanostructured Li2S/silicon rechargeable battery with high specific energy. *Nano Lett* 10:1486–1491.
46. Cui L-F, Yang Y, Hsu C-M, Cui Y (2009) Carbon-silicon core-shell nanowires as high capacity electrode for lithium ion batteries. *Nano Lett* 9:3370–3374.